IEEE Access
Multidisciplinary | Rapid Review | Open Access Journal

Received February 19, 2019, accepted February 26, 2019, date of publication March 12, 2019, date of current version March 29, 2019.

Digital Object Identifier 10.1109/ACCESS.2019.2904051

A Tunable MIMO Antenna With Dual-Port Structure for Mobile Phones

WON-WOO LEE[1] AND BEAKCHEOL JANG[2], (Member, IEEE)
[1]ICT Convergence Research Division, Korea Expressway Corporation Research Institute, Hwaseong 18489, South Korea
[2]Department of Computer Science, Sangmyung University, Seoul 03016, South Korea

Corresponding author: Beakcheol Jang (bjang@smu.ac.kr)

ABSTRACT In this paper, we develop a new frequency reconfigurable dual-port antenna that has two independent signal feed ports in a single antenna element for multiple-input multiple-output capable mobile handsets. The proposed antenna is composed of a cross-coupled semi-loop (CCSL) structure with a single pole 4-throw controlled by a logic circuit for frequency tuning capability and a Planar Inverted-F Antenna (PIFA) with a coupled pattern for wideband characteristics. The operating frequency ranges are 2.5–3.6 GHz, which corresponds to Band 7 (2500–2690 MHz), Band 22 (3410–3590 MHz), Band 38 (2570–2620 MHz), Band 41 (2496–2690 MHz), and Band 42 (3400–3600 MHz). The good isolation between the two signal input ports is achieved due to the CCSL radiator which creates orthogonal current flow direction with respect to the current induced by the PIFA radiator. The parametric study results of the dual-port antenna are presented to explain the optimization process based on the simulation works and experiments. We show that the proposed dual-port antenna has frequency tuning ranges up to 800 MHz while maintaining the port-to-port isolation greater than 10 dB.

INDEX TERMS Antenna, ECC, LTE, MIMO, dual-port.

I. INTRODUCTION

The most important requirement of the Multiple-Input Multiple-Output (MIMO) [1]–[3] antenna system for smartphones have been a multi-band operation, low antenna correlation [4]–[7], and compact size [8], [9]. Due to the needs for the scale of economy, the device manufacturers must reduce the number of hardware components and this demands an increased number of frequency bands using simpler hardware. New smartphones on the global markets have to support more than 16 different frequency bands including global roaming bands [10]. Furthermore, additional receive antennas are required to support 4×4 MIMO, and the challenges to the size of the MIMO antennas become greater than ever.

To overcome these problems, several studies proposed dual-port antennas based on Planar Inverted-F Antenna (PIFA) to reduce the total volume of the antenna [11]–[16]. The study in [11] studied the antenna correlation characteristics of a dual-port antenna with two feed ports placed perpendicularly to each other to exploit both the polarization diversity and pattern diversity, and studies on [12], [13] further optimized the size. However, these studies had drawbacks in the realization of the real device form factors due to the size and the special requirement for the shape of the ground plane. These studies also revealed that the port-to-port isolation was the main drawback of PIFA or IFA based dual-port antennas. The study in [14] discovered that the proposed hybrid antenna array elements are symmetrically placed along the long edges of the smartphone, and they are composed of two different four-antenna array types, C-shaped coupled-fed and L-shaped monopole slot, that exhibit orthogonal polarization. The study in [15] proposed a neutralization line (NL) for port decoupling in smartphone applications. The U-shape NL is employed to achieve enhanced isolations for the lower band. These studies implemented dual port antennas to put physically separated antennas together, but they were too large to implement on smartphones. The study in [16] proposed an integrated yet decoupled (IYD) dual antennas with inherent decoupling structures to achieve MIMO operation in the 2.4/5.2/5.8-GHz wireless local area network bands. The IYD dual antennas consist of two coupled-fed loop antennas integrated into a compact planar structure. The proposed antenna was a good solution for the dual port antenna, even though it was not suitable for low band solution.

In this paper, we propose a more size-efficient, low cost and frequency reconfigurable dual-port MIMO antenna. A PIFA

The associate editor coordinating the review of this manuscript and approving it for publication was Lin Peng.

with a coupled pattern and the cross-coupled semi-loop (CCSL) antenna are merged to form a dual-port antenna. The advantage of using the CCSL is that a good isolation between the two signal feeding ports can be achieved because of its sensitivity to the magnetic field, whereas the PIFA is more sensitive to the electric field. For frequency tuning capability, a single pole 4 throws (SP4T) RF switch [17] is used to the ground short pin of the dual-port antenna for load impedance switching [18]. Lumped components are used to provide impedance switching on both the PIFA branch and CCSL, so the operating frequency ranges of both signal input ports are 2.5 GHz - 3.6 GHz [19]. To our best knowledge, there have been no such results reported so far on the frequency reconfigurable dual-port antennas. It is a great advantage for dual-port antenna to applying a single RF switch to achieve the frequency tuning on the two antenna branches, because it saves both the cost and the complexity of antenna design. The big challenge to deal with is the frequency tuning of the two antenna elements to the same direction using the same load impedances while keeping a good isolation between two signal ports. Optimization of the antenna is done in a way that PIFA element is wideband so that it covers the frequency tuning ranges of the CCSL. The achieved isolation between the PIFA branch and the CCSL is below 12 dB and the measured envelope correlation coefficient (ECC) is below 0.16 across the operating frequency ranges. We present comparative analysis results including the parametric studies on the antenna properties of the proposed dual-port antenna, and the results are applied to fabricate a mock-up antenna to exploit the characteristics of the dual-port antenna through measurements.

The remainder of this paper is organized as follows. Section II presents dimensions and prototyping of antennas. In Section III and IV, we demonstrate computer simulation and experimental measurements. Finally, we conclude in Section V.

II. ANTENNA DESIGN

This section presents the structural details of the proposed dual-port antenna design with dimensional information and topology. We explain the design approaches to achieve a good isolation between two radiators and the frequency tuning scheme. Different from the previous studies on the dual-port antennas [12], [13], [17] where two PIFAs are merged or a single element PIFA plate with two feeding ports are used, we combine two different types of antenna topologies to form a dual-port antenna, which is the key to achieve a good port-to-port isolation.

Fig. 1 shows a mock-up antenna to evaluate the characteristics of the dual-port MIMO antenna. The size of the PCB board is 60 × 100 × 1 mm^3, and it is printed on the top of an FR4 substrate. The overall antenna PCB circuit height is 1.3mm, considering the SP4T RF switch component size (3mm × 3mm × 0.6mm) on the front side direction and voltage component size (2.1mm × 2.1mm × 0.7mm) on the rear side direction. The antenna patterns are located

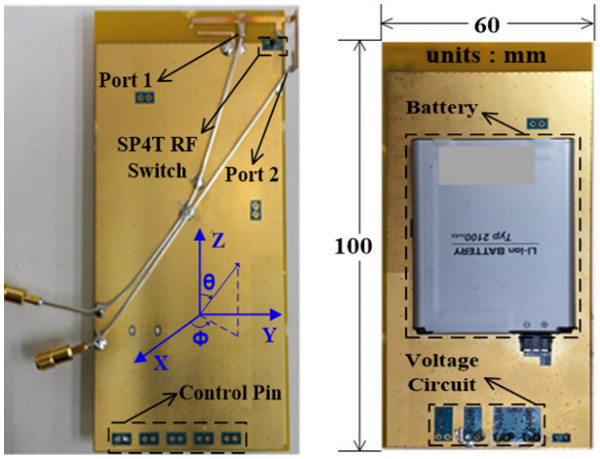

FIGURE 1. Photography of prototype MIMO antenna, (a) Front side (b) rear side.

at the bottom of the front side of the PCB, and an SP4T RF switch is mounted near the ground short pin of the antenna for impedance switching. To keep a smaller volume, the CCSL and the signal port 2 are folded by 90 degrees perpendicularly to the PCB board. The overall dimensions of the antenna are 27.5 × 8 mm2 for PIFA part and 10 × 17.3 mm2 for CCSL part. These dimensions are compact enough to fit in mobile handsets. To facilitate measurements, 50ohm-shielded semi-rigid cables with SMA connectors are connected to both signal feed ports of the dual-port antenna as shown in Fig. 1 (a). DC bias circuitries and a Li-ion battery as a power supply of SP4T are mounted on the back side of the PCB board as shown in Fig. 1 (b).

As shown in Fig. 2. a PIFA is used to realize signal port 1 and the ground. The primary signal port (port 1) is branched from the radiator just as a normal PIFA. A coupling slot placed in parallel to the PIFA is used to enhance the operating bandwidth by creating the second resonance at 3.5 GHz. An inverted L-shaped branched out from the ground short of

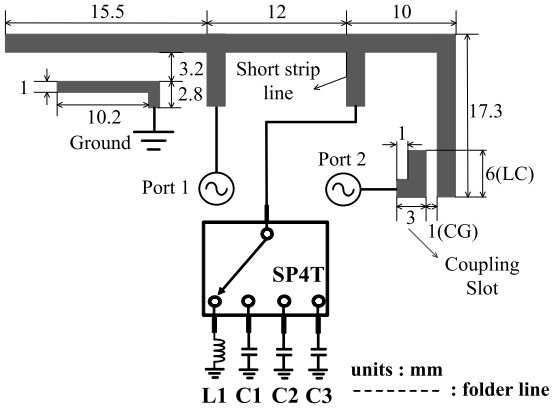

FIGURE 2. Schematic of the tunable dual-port MIMO antenna with dimensional information.

the PIFA is the secondary radiator and the coupled signal feed port 2 comprise the CCSL in Fig. 2.

The output port of the SP4T RF switch is connected to the ground short and the four input ports are connected to the four different lumped components. The impedance tuning of the antenna can be done by switching the connected load impedances. Table 1 shows the four different frequency tuning states of the dual-port antenna and associated lumped component values.

TABLE 1. SP4T operation table of dual-port antenna.

Service band [1]	frequency of CCSL [GHz]	Control 1	Control 2	Value
Band 7/38/41	2.6	LOW	LOW	L1(2.2nH)
-	2.8	HIGH	LOW	C1(100pF)
-	3.1	LOW	HIGH	C2(0.5pF)
Band 22/42	3.4	HIGH	HIGH	C3(0.1pF)

The center frequency of PIFA is not presented because of its wideband property

The tuning range is between 2.5 – 3.6 GHz along with the load impedance value changes from L1 to C3 in table 1. The center frequencies of CCSL are only presented because there is no change in the resonance frequency of PIFA depending on the load impedance values. The physical lengths for both radiators are optimized at 3.4 GHz with the load impedance of C3 (0.1 pF).

By using L1 (2.2 nH), the center frequency of the CCSL is tuned to 2.6 GHz and the bandwidth of the PIFA is extended down to 2.5 GHz covering 3GPP band 7, 38 and 41. The PIFA is designed in a way that its bandwidth covers up to 3.6 GHz regardless of the load impedance values.

III. SIMULATION

A. CURRENT DISTRIBUTIONS

The induced current distributions in the PCB board excited by the two antenna elements are simulated and illustrated in Fig. 3. For the simulation section and the parametric studies on the dimensional changes of the proposed antenna, we used computer simulation technology (CST) MICROWAVE STUDIO 2016 [20]. Fig. 4 shows the current distributions on the PCB induced by the dual-port antenna at 2.5 and 3.5 GHz when the two signal ports are simultaneously excited. At 2.5 GHz, it is observed that the currents between the two ports are not highly concentrated when both ports are excited. It suggests that good port to port isolation characteristics can be expected. At the 3.5 GHz band, the current flowing between the two ports is slightly increased as the current density at each signal port is increased compared with the case of the 2.5 GHz band.

Fig. 4 demonstrates the directions of the simulated current flows on the ground plane and the radiating patterns when both signal ports are excited. The directions of the current

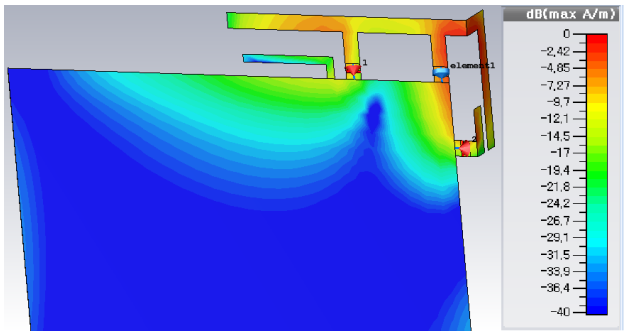

(a)

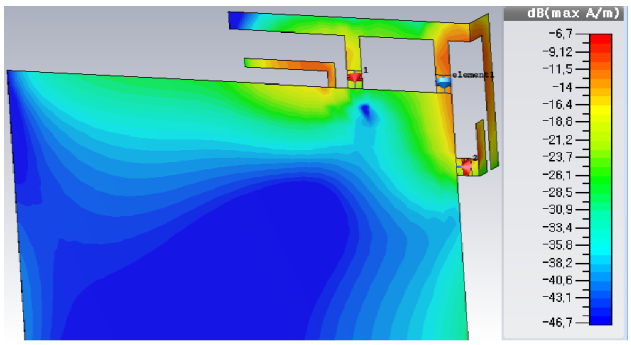

(b)

FIGURE 3. Simulated current distributions when two ports are excited simultaneously, (a) at 2.5GHz (b) at 3.5GHz.

flows created by each signal port are clearly different. The largest current flow from the primary signal (port 1) is in the horizontal direction, whereas that of the secondary signal (port 2) is in the vertical direction.

The similar observations can be seen at both frequency bands. Such orthogonality in the direction of the current flows between the two signal ports is the key aspect of achieving good isolation between two signal ports. When we compare the current flow at different frequency bands, the hot spots are closer to the feeding port for 3.5 GHz band whereas those for the 2.5 GHz band are near the radiators. Particularly at 3.5 GHz, the current densities near the coupled pattern are larger than at the PIFA radiator which provides additional isolation between two signal ports.

B. PARAMETRIC STUDY

To optimize the performance of the dual-port antenna, we studied on the variations in lengths of the coupling pattern (LC) for CCSL and the gap in between coupling gap (CG). The parameters, LC and CG are illustrated in Fig. 2. Fig. 5 and 6 show the simulated S-parameters for each signal port of dual-port antenna with respect to the length of the signal port 2 pattern (LC) and the CG as presented in Fig. 2. For the simulations, load impedance is set to 2.2 nH to configure the operating frequency to its lowest frequency (e.g., 2.5 GHz).

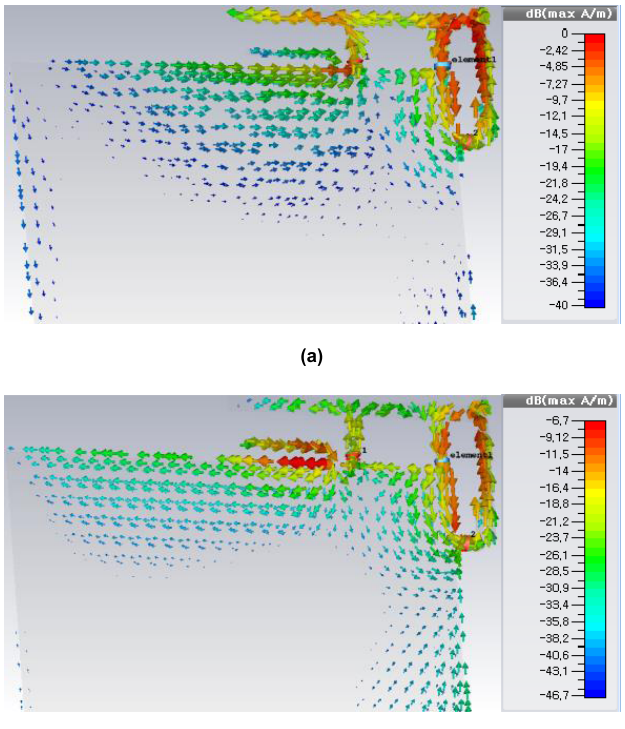

FIGURE 4. Simulated current flows when two ports are excited simultaneously, (a) at 2.5GHz (b) at 3.5GHz.

In Fig. 5 (b), LC is varied from 2 – 10 mm and CG is fixed at 1.0 mm, which shifts the resonance frequency of CCSL element from 2.65 to 2.4 GHz. In Fig. 6 (b), the resonance frequency of the CCSL element varies from 2.5 to 2.15 GHz, as the CG is changed from 1.6 mm to 0.4 mm. This can be explained that the coupling pattern is a parasitic load capacitance seen by the CCSL radiator, and its value is proportional to LC but inversely proposal to CG. Therefore, the resonance frequency is detuned to the lower frequency as LC increases, and CG decreases. Note that changes of LC and CG do not impact on the S-parameters of the primary radiator as shown in Fig. 5 (a) and 6 (a).

Based on the simulation results, it is concluded that the LC should be at least 6 mm and GC needs to be 0.7∼1.5 mm to achieve good resonance characteristics. For the prototyped antenna, 1 mm is chosen for GC for the sake of simplicity and scalability of tooling the antennas in a lab environment and use 6 mm of LC for resonance at 2.5 GHz. The same optimization procedure has been done for PIFA and its coupling pattern.

Fig. 7 shows the simulated isolation properties between two signal ports for several different LC-GC combinations which are chosen to keep the resonance frequency of the CCSL at 2.5 GHz. Note that the isolation near 2.5 GHz decreases as the LC increases and this tells that LC should not be too long. Recalling that the minimum LC is 6 mm to achieve a good resonance characteristic, 6mm of LC and 1 mm of CG can be an optimal value for prototype antenna realization.

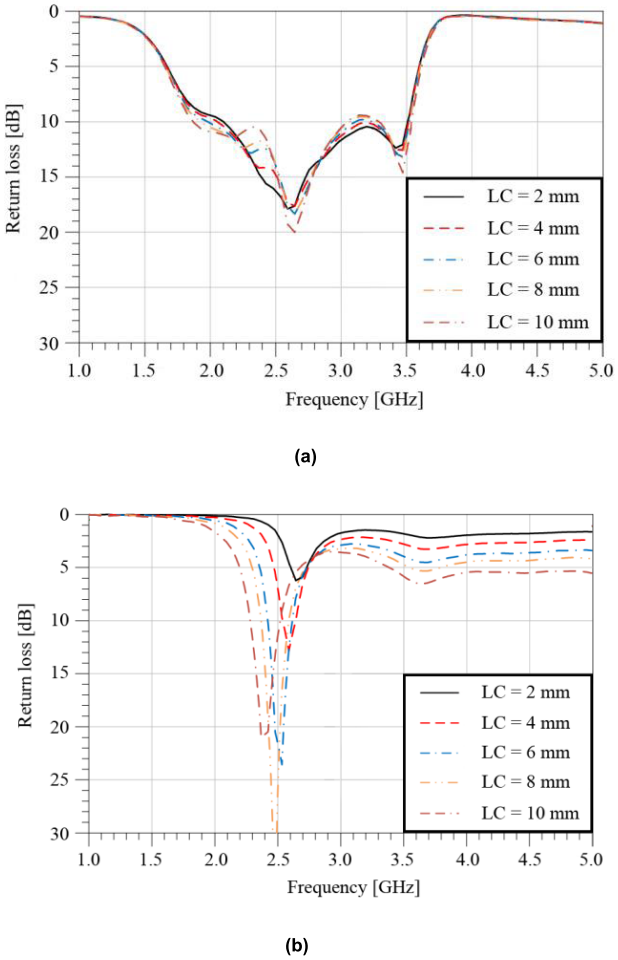

FIGURE 5. Simulated S-parameters for various LC values (length of the signal port 2 pattern). CG is fixed at 1.0 mm. (a) S11 (port 1), (b) S22 (port 2).

IV. RESULTS AND DISCUSSIONS

A. S-PARAMETERS

Fig. 8 shows the simulated and measured S-parameters of the prototyped dual-port MIMO antenna with different switching load impedance values presented in Table 1. The antenna is realized based on the dimensions illustrated in Fig. 2. Both the measured and simulated results are shown together for comparison purpose. Depending on the switching states of the SP4T, CCSL radiator shows distinctive changes of the resonance frequencies but PIFA experiences only a slight change of operating bandwidth. It is observed that the tuning range of the CCSL with a selection of load impedance values between 2.2 nH and 0.1 pF is around 27 % near 2.6 GHz as shown in Fig. 9 (b). In fact, the bandwidth of the PIFA is extended down to 2.5 GHz with the load impedance value of 2.2 nH by which the CCSL is tuned to 2.5 GHz. In this way, both antenna elements are tuned to the same direction covering 2.5 – 3.6 GHz with only a single RF switch.

Fig. 8 (c) shows the isolation properties between the two signal ports, and it shows 12 dB at 2.5 GHz and 15 dB at 3.5GHz suggesting the prototyped antenna can be used for MIMO applications. It is also noted that the measurement

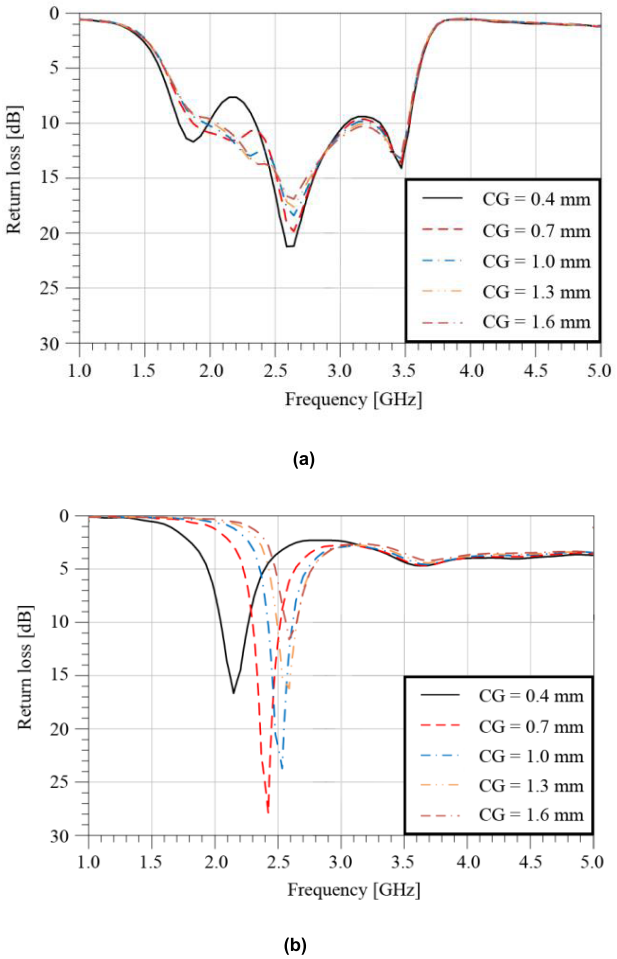

FIGURE 6. Simulated S-parameters for various CG (coupling gap between the signal port 2 pattern and CCSL). LC is fixed at 6 mm. (a) S11 (port 1), b) S22 (port 2).

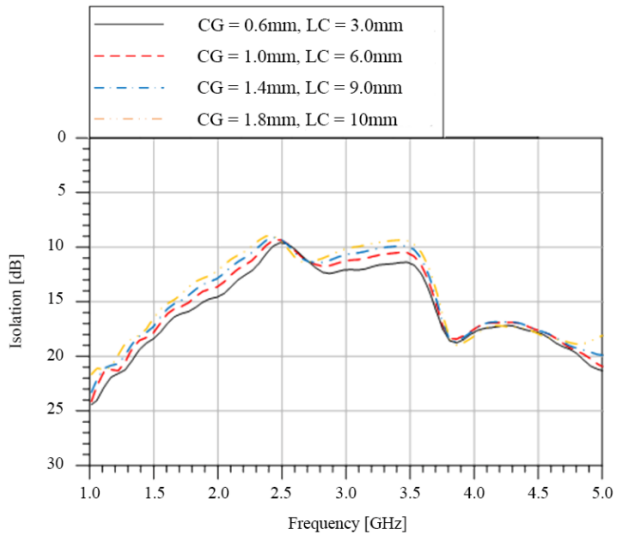

FIGURE 7. Simulated S21 for various CG-LC combinations.

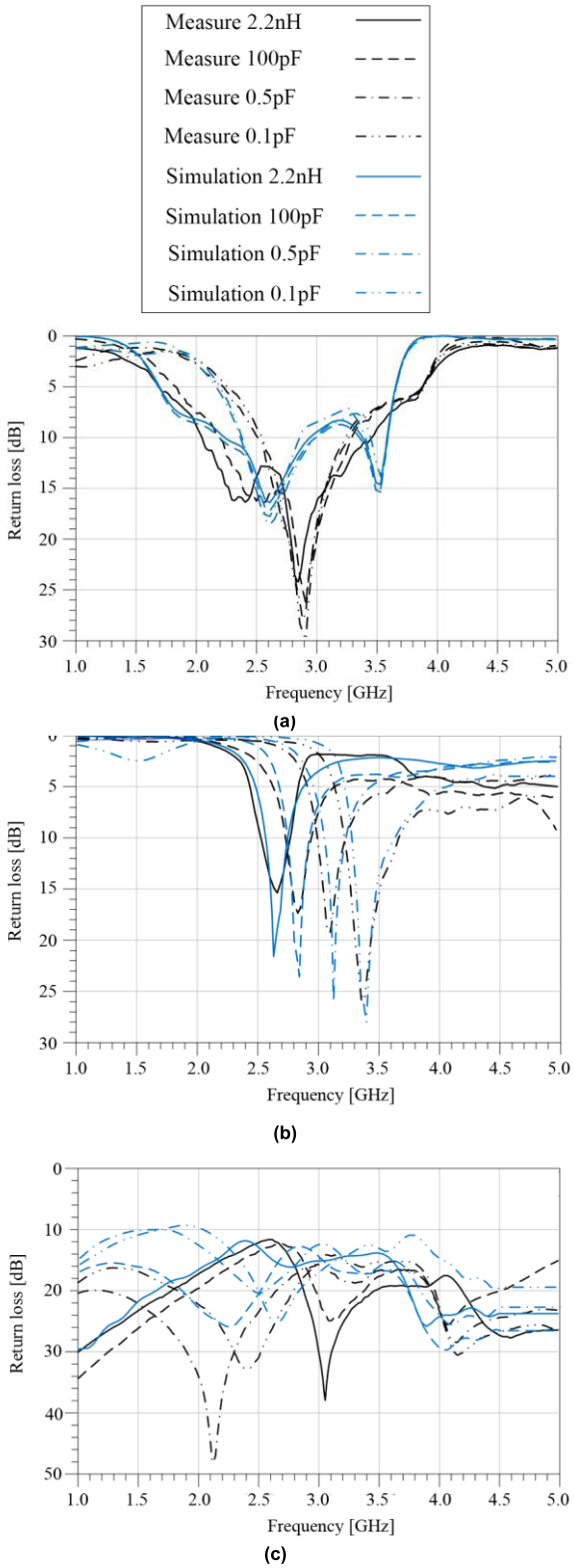

FIGURE 8. Simulated and measured S-parameter for the prototyped antenna, (a) S11 (port 1), (b) S22 (port 2), (c) S21 (port 1 - port 2).

results have a good agreement with the simulation results in general. The slight differences exist because of coherency and manufacturing tolerance.

B. RADIATION PATTERN

The radiation patterns (total electric-field) of the prototyped antenna are measured using Microwave Technologies Group

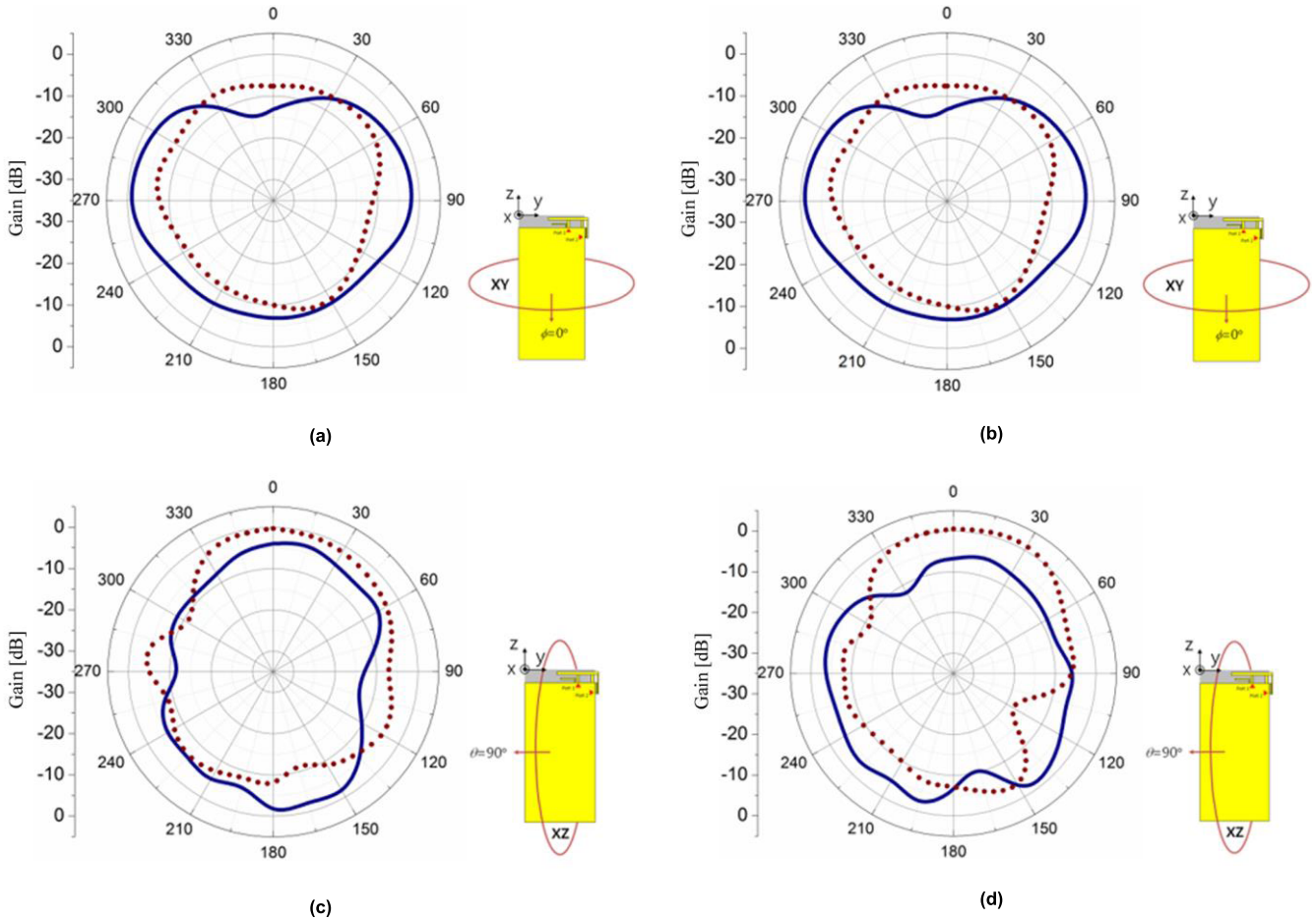

FIGURE 9. Measured 3-D radiation patterns of the prototyped antenna, (a) X-Y plane at 2.5GHz, (b) X-Y plane at 3.5GHz, (c) X-Z plane at 2.5GHz, (d) X-Z plane at 3.5GHz.

version 2.1 (MTG ver.2.1), a 3D measurement tool [21]. The radiation patterns of the antenna are measured when one port is fed at a time while the other port is terminated with a 50-load. The measured radiation patterns at 2.4 and 3.5 GHz are shown in Fig. 9. The radiation patterns of the PIFA (port 1) in the x-y plane are not symmetrical but directional at 90 and 270 as shown in Fig. 9(a) and (b). However, the radiation patterns of the CCSL (port 2) in the x-y plane are rather symmetrical than those of PIFA. At 2.5 GHz, the radiation pattern of CCSL is smaller than that of at 3.5 GHz because the original operating frequency of the CCSL element is tuned at 3.5 GHz with the load impedance value of 0.5 pF. Both the PIFA and CCSL radiation patterns are directional at 90 and 270 at 3.5 GHz and are very similar to each other in their shapes. The radiation patterns in the x-z plane show that both the PIFA and CCSL elements are directional around $\theta = 0°$ at 2.5 GHz but only CCSL is directional around $\theta = 90°$ in case of 3.5 GHz.

Fig. 10 shows the measured total gain of the prototyped antenna. The gain curves for both radiators are measured for the cases of load impedance value of 2.2 nH and 0.1 pF. PIFA radiator shows only a slight gain enhancement with

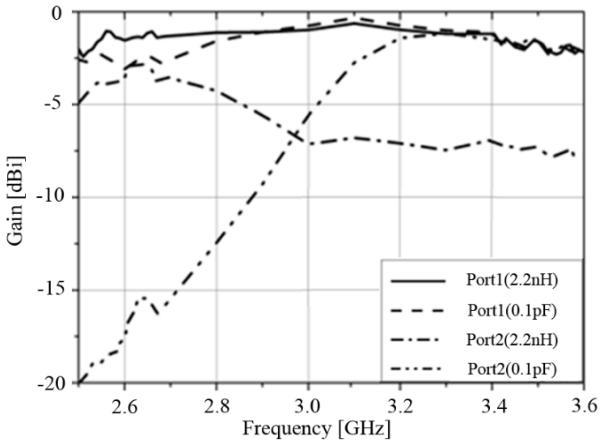

FIGURE 10. A measured total gain of a prototyped antenna with different load impedance values.

2.2 nH compared with 0.1 pF load impedance. The PIFA shows gain ranges of about −2.0 dBi at 2.5 GHz and −1.7 dBi at 3.5 GHz. In the case of the CCSL radiator, the gain curves

$$\rho_{12} = \frac{\left| \oint \{XPR \cdot E_{\theta 1}(\Omega) \cdot E^*_{\theta 2}(\Omega) + E_{\emptyset 1}(\Omega) \cdot E^*_{\emptyset 2}(\Omega)\} d\Omega \right|^2}{\oint \{XPR \cdot G_{\theta 1}(\Omega) + G_{\emptyset 1}(\Omega)\} d\Omega \cdot \oint \{XPR \cdot G_{\theta 2}(\Omega) + G_{\emptyset 2}(\Omega)\} d\Omega} \quad (1)$$

are distinctively tuned by the load impedance changes. The gain ranges are −4.9 dBi at 2.5 GHz and −1.9 dBi at 3.5 GHz. The smaller gain at 2.5 GHz is due to the degraded matching observed in the measured S-parameter results of Fig. 8 (b). This is because the operating frequency is far away from the initial resonance frequency of the antenna. However, gain differences between the two radiators are still within an acceptable range considering the corresponding requirement from one of the major LTE service operators in the U.S [22].

C. ENVELOPE CORRELATION COEFFICIENT

Fig. 11 shows ECC for the prototyped dual-port antenna based on the measured radiation patterns [23]. Under the assumption of uniformly scattered radio environments, ECC between two antennas can be derived from equation (1), as shown at the top of this page, and complex radiation patterns.

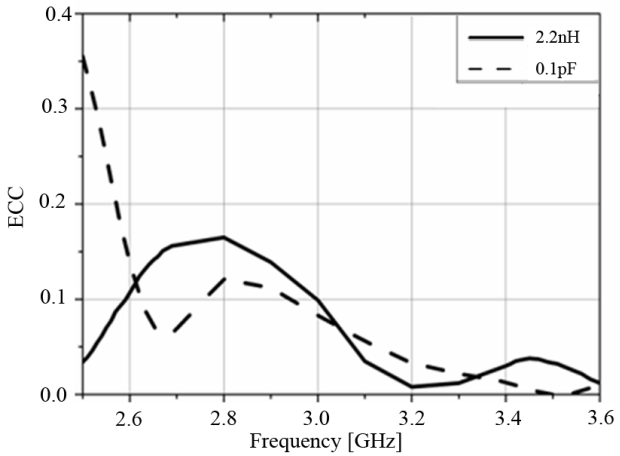

FIGURE 11. Measured ECC characteristics with tuning impedance value of 2.2 nH and 0.1 pF.

Eθ1(Ω) and EØ1(Ω) denote the vertical and the horizontal polarization complex radiation patterns for the PIFA element. Eθ2(Ω) and EØ2(Ω) are the vertical and the horizontal polarized complex radiation patterns for the CCSL element. Ω denotes the solid angle in the spherical coordinate system. XPR = 1 if the channel is isotropic.

With the tuning impedance value of 2.2 nH, the ECC varies from 0.04 to 0.16 at Band 7 (2.5-2.69 GHz). The ECC drops down below 0.02 at Band 42 (3.4-3.6 GHz) with the tuning impedance value of 0.1 pF. The ECC measurement results tell that the proposed dual-port antenna can be an alternative solution for MIMO antenna applications for the mobile handsets.

V. CONCLUSIONS

In this paper, we present a new type of dual-port MIMO antenna based on merged PIFA and CCSL and demonstrated its characteristics. The operating frequency ranges of the dual-port antenna are 2.5-3.6 GHz. The key advantages of the proposed antenna are a small size, high isolation, and low cost. The wideband operation is achieved by adopting an SP4T that switches four different lumped inductor or capacitors for the frequency detuning. Through the simulations, we show that a good port-to-port isolation is achieved due to the orthogonal current distributions created by each element and it is confirmed through the measured S-parameters and ECC. Through this study, it is proven that the proposed frequency reconfigurable dual-port MIMO antenna can be an alternative solution for the higher order MIMO under 6 GHz frequency ranges as well as the 5th generation mobile broadband standard that requires many frequency bands.

REFERENCES

[1] D. Gesbert, M. Shafi, D.-S. Shiu, P. J. Smith, and A. Naguib, "From theory to practice: An overview of MIMO space-time coded wireless systems," *IEEE J. Sel. Areas Commun*, vol. 21, no. 3, pp. 281–302, Apr. 2003.

[2] E. G. Larsson, O. Edfors, F. Tufvesson, and T. L. Marzetta, "Massive MIMO for next generation wireless systems," *IEEE Commun. Mag.*, vol. 52, no. 2, pp. 186–195, Feb. 2014.

[3] S. Shoaib, I. Shoaib, N. Shoaib, X. Chen, and C. G. Parini, "MIMO antennas for mobile handsets," *IEEE Antennas Wireless Propag. Lett.*, vol. 14, pp. 799–802, 2015.

[4] P. Vainikainen *et al.*, "Recent development of mimo antennas and their evaluation for small mobile terminals," in *Proc. 17th Int. Conf. Microw., Radar Wireless Commun.*, May 2008, pp. 1–10.

[5] T. Ohishi, N. Oodachi, S. Sekine, and H. Shoki, "A method to improve the correlation coefficient and the mutual coupling for diversity antenna," in *Proc. IEEE Antennas Propag. Soc. Int. Symp.*, vol. 1A, Jul. 2005, pp. 507–510.

[6] A. Diallo, C. Luxey, P. L. Thuc, R. Staraj, and G. Kossiavas, "Study and reduction of the mutual coupling between two mobile phone PIFAs operating in the DCS1800 and UMTS bands," *IEEE Trans. Antennas Propag.*, vol. 54, no. 11, pp. 3063–3074, Nov. 2006.

[7] A. C. K. Mak, C. R. Rowell, and R. D. Murch, "Isolation enhancement between two closely packed antennas," *IEEE Trans. Antennas Propag.*, vol. 56, no. 11, pp. 3411–3419, Nov. 2008.

[8] F. Jianli, M. Jie, and Z. Xiaomin, "Compact octa-band PIFA for LTE/GSM/UMTS/WLAN operation in the mobile," in *Proc. 5th Int. Conf. Intell. Syst. Des. Eng. Appl.*, Hunan, China, Jun. 2014, pp. 296–299.

[9] Z. Ying and D. Zhang, "Study of the mutual coupling, correlations and efficiency of two PIFA antennas on a small ground plane," in *Proc. IEEE Antennas Propag. Soc. Int. Symp.*, Washington, DC, USA, Jul. 2005, pp. 305–308.

[10] *LTE Frequency Bands*. Accessed: Mar. 14, 2019. [Online]. Available: https://en.wikipedia.org/wiki/LTE_frequency_bands

[11] H. T. Chattha, S. J. Boyes, Y. Huang, and X. Zhu, "Polarization and pattern diversity-based dual-feed planar inverted-f antenna," *IEEE Trans. Antennas Propag.*, vol. 60, no. 3, pp. 1532–1539, Mar. 2012.

[12] H. T. Chattha, M. Nasir, Q. H. Abbasi, Y. Huang, and S. S. AlJa'afreh, "Compact low-profile dual-port single wideband planar inverted-f MIMO antenna," *IEEE Antennas Wireless Propag. Lett.*, vol. 12, pp. 1673–1675, 2013.

[13] Q. Rao and D. Wang, "A compact dual-port diversity antenna for long-term evolution handheld devices," *IEEE Trans Veh. Technol.*, vol. 59, no. 3, pp. 1319–1329, Mar. 2010.
[14] M.-Y. Li *et al.*, "Eight-port dual-polarized MIMO antenna for 5G smartphone applications," *IEEE Trans. Antennas Propag.*, vol. 64, no. 9, pp. 3820–3830, Sep. 2016.
[15] Y.-L. Ban, Z.-X. Chen, Z. Chen, K. Kang, and J. L.-W. Li, "Decoupled hepta-band antenna array for WWAN/LTE smartphone applications," *IEEE Antennas Wireless Propag. Lett.*, vol. 13, pp. 999–1002, 2014.
[16] K.-L. Wong, C.-Y. Tsai, and W.-Y. Li, "Integrated yet decoupled dual antennas with inherent decoupling structures for 2.4/5.2/5.8-GHz WLAN MIMO operation in the smartphone," *Microw. Opt Technol Lett.*, vol. 59, no. 9, pp. 2235–2241, 2017.
[17] Qorvo company. Accessed: Mar. 14, 2019. [Online]. Available: https://www.qorvo.com/
[18] W.-W. Lee and Y.-S. Cho, "Frequency tunable antenna using coupling patterns for mobile terminals," *Electron. Lett.*, vol. 51, no. 22, pp. 1725–1726, Oct. 2015.
[19] *Evolved Universal Terrestrial Radio Access (E-UTRA); User Equipment (UE) Radio Transmission and Reception*, document 3GPP TS 36.101, 2017. [Online]. Available: http://www.3gpp.org/ftp/Specs/html-info/36101.htm
[20] *Computer Simulation Technology (CST) Microwave Studio Suite 2016*. Accessed: Mar. 14, 2019. [Online]. Available: http://www.cst.com
[21] MTG company. *Microwave Technologies Group*. Accessed: Mar. 14, 2019. [Online]. Available: http://mtginc.co.kr/
[22] Verizon company. Accessed: Mar. 14, 2019. [Online]. Available: https://opendevelopment.verizonwireless.com/
[23] I. Szini, G. F. Pedersen, S. C. D. Barrio, and M. D. Foegelle, "LTE radiated data throughput measurements, adopting MIMO 2x2 reference antennas," in *Proc. IEEE Veh. Technol. Conf. (VTC Fall)*, Sep. 2012, pp. 1–5.

WON-WOO LEE received the B.S. degree in electronics and physics from Kwangwoon University, South Korea, in 2000, the M.S. degree in microwave engineering from Kwangwoon University, in 2002, and the Ph.D. degree in electrical and computer engineering from Hanyang University, in 2014. He is currently with the ICT Convergence Research Division, Korea Expressway Corporation Research Institute. His research interests include the area of design and analysis of LTE systems, 5G mmWave systems, and antenna and microwave circuit design.

BEAKCHEOL JANG received the B.S. degree from Yonsei University, in 2001, the M.S. degree from the Korea Advanced Institute of Science and Technology, in 2002, and the Ph.D. degree from North Carolina State University, in 2009, all in computer science. He is currently an Associate Professor with the Department of Computer Science, Sangmyung University. His current research interests include wireless networking, big data, the Internet of Things, and artificial intelligence. He is a member of the ACM.